PLOS ONE

RESEARCH ARTICLE

A computational modelling framework to quantify the effects of passaging cell lines

Wang Jin, Catherine J. Penington, Scott W. McCue, Matthew J. Simpson*

School of Mathematical Sciences, Queensland University of Technology (QUT) Brisbane, Queensland 4000, Australia

* matthew.simpson@qut.edu.au

Check for updates

OPEN ACCESS

Citation: Jin W, Penington CJ, McCue SW, Simpson MJ (2017) A computational modelling framework to quantify the effects of passaging cell lines. PLoS ONE 12(7): e0181941. https://doi.org/10.1371/journal.pone.0181941

Editor: Grant Lythe, University of Leeds, UNITED KINGDOM

Received: May 18, 2017

Accepted: July 10, 2017

Published: July 27, 2017

Copyright: © 2017 Jin et al. This is an open access article distributed under the terms of the Creative Commons Attribution License, which permits unrestricted use, distribution, and reproduction in any medium, provided the original author and source are credited.

Data Availability Statement: All relevant data are within the paper and its Supporting Information files.

Funding: This work is funded by the Australian Research Council (Grants: DP140100249 to MJS and SWM, DP170100474 to MJS; http://www.arc.gov.au/). The funders had no role in study design, data collection, decision to publish, or preparation of the manuscript.

Competing interests: The authors have declared that no competing interests exist.

Abstract

In vitro cell culture is routinely used to grow and supply a sufficiently large number of cells for various types of cell biology experiments. Previous experimental studies report that cell characteristics evolve as the passage number increases, and various cell lines can behave differently at high passage numbers. To provide insight into the putative mechanisms that might give rise to these differences, we perform *in silico* experiments using a random walk model to mimic the *in vitro* cell culture process. Our results show that it is possible for the average proliferation rate to either increase or decrease as the passaging process takes place, and this is due to a competition between the initial heterogeneity and the degree to which passaging damages the cells. We also simulate a suite of scratch assays with cells from near–homogeneous and heterogeneous cell lines, at both high and low passage numbers. Although it is common in the literature to report experimental results without disclosing the passage number, our results show that we obtain significantly different closure rates when performing *in silico* scratch assays using cells with different passage numbers. Therefore, we suggest that the passage number should always be reported to ensure that the experiment is as reproducible as possible. Furthermore, our modelling also suggests some avenues for further experimental examination that could be used to validate or refine our simulation results.

Introduction

In vitro cell culture is routinely used to grow and supply cells for various types of cell biology experiments [1]. These experiments are used to study a wide range of biological phenomena including drug design, cancer spreading and tissue repair [2–5]. According to the American Type Culture Collection (ATCC) protocols, to grow cells in traditional two–dimensional (2D) *in vitro* cell culture, cells propagated in a growth medium are initially seeded as a monolayer in a cell culture flask [6], as shown in Fig 1a. Cells are seeded in a monolayer with a density typically varying from 10–20% of confluence [6]. Cells are then cultured in an incubator, in an appropriate temperature and CO_2 concentration, and grown until they reach a density of 80%–90% of confluence [6]. To continue growing the population, cells are lifted, often using trypsin, and spilt into smaller proportions. The smaller subpopulations are transferred into new cell culture flasks to re-grow [6]. This process is referred to as *passaging*, with passage

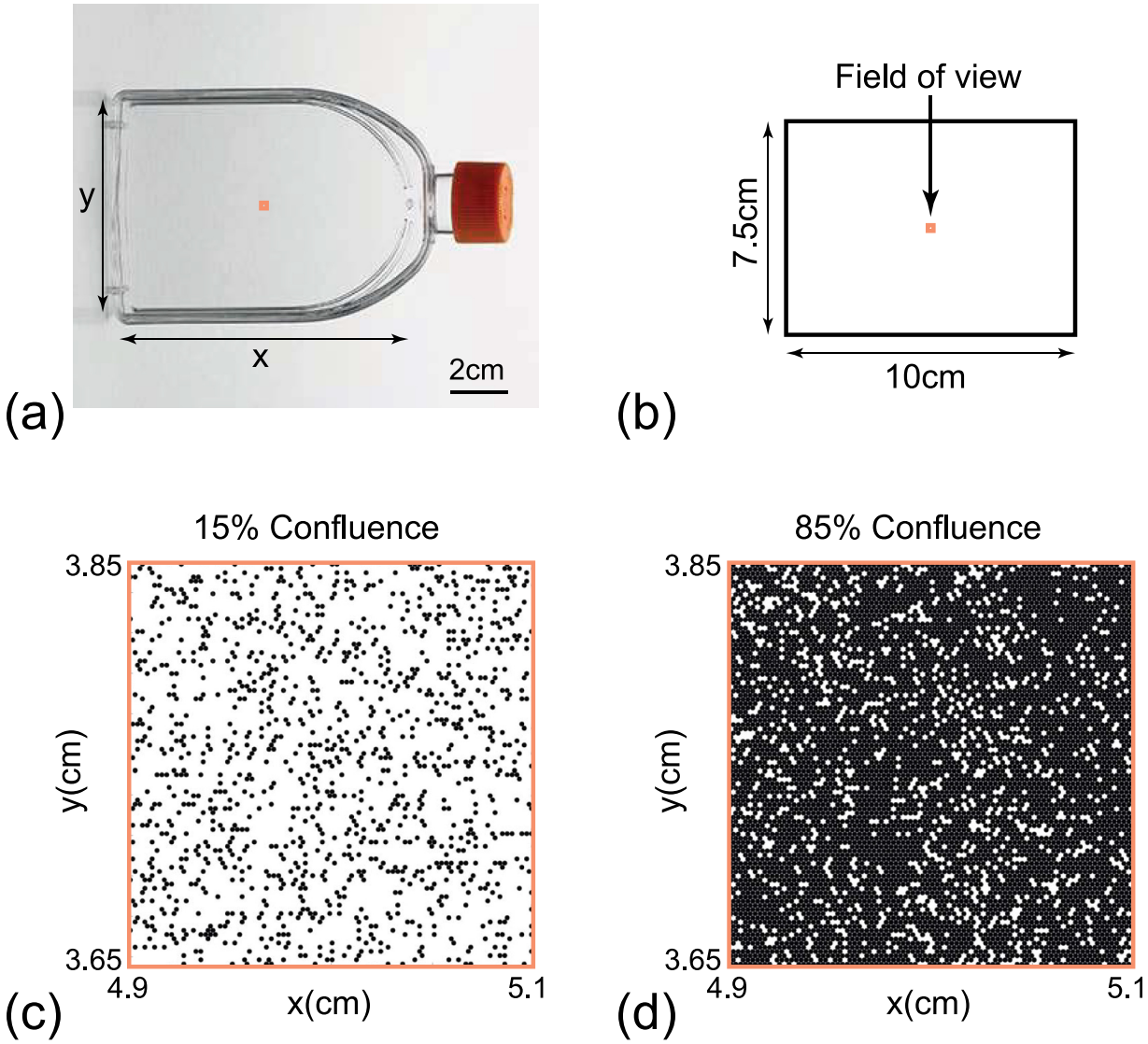

Fig 1. Schematic illustration of the simulation domain. (a) Photograph of a 75 cm^2 cell culture flask. (b) Schematic of the 10 cm × 7.5 cm simulation domain that represents the 75 cm^2 flask. The orange squares in (a) and (b) indicate the 2 mm × 2 mm field of view. (c) Snapshot of the field of view at 15% confluence. (d) Snapshot of the field of view at 85% confluence.

https://doi.org/10.1371/journal.pone.0181941.g001

number indicating the number of splits [6, 7]. Although passaging is a standard process in 2D cell culture, the passage number of cells used in experiments is not always reported in experimental protocols [8–13].

It is known that passaging can affect cells in a number of ways, and therefore has the potential to impact the reproducibility of *in vitro* experiments [12]. There are many ways in which passaging can affect cells. For example, primary cells, which are directly isolated from living tissues [14], undergo morphological changes and cumulative damage as the passage number increases [15–22]. As a result, the cell morphology, migration rate and proliferation rate can become increasingly varied, which is thought to increase the heterogeneity in cell lines [16, 17, 19, 21, 22]. Because a range of cell behaviours could depend on passage number, the passaging process can be a source of variability that affects the reproducibility of various *in vitro* experiments, such as 2D scratch assays [7, 12, 13].

Seemingly contradictory observations have been reported about the effects of passaging cell lines [16, 17, 21–23]. For example, Hayflick reports that for human diploid cell lines, cells at high passage numbers demonstrate increased generation time, gradual cessation of mitotic activities, and accumulation of cellular debris [17]. This observation of decreased cell proliferation rate is also supported by studies of other cell lines [16, 21, 22]. However, Lin and coworkers show that the population of LNCaP cells at passage number 70 is over two times larger than that at passage number 38 after five days [23]. It has also been stated that for some cell lines, changes due to the passaging process occur at relatively low passage numbers, whereas for other cell lines the changes occur at relatively high passage numbers [7]. Therefore, we are motivated to undertake a mechanistic study to quantify how different variables relevant to the passaging process might give rise to such seemingly contradictory observations and to explore how these effects might impact the reproducibility of *in vitro* experiments.

Although problems associated with high passage numbers are widely acknowledged, the mechanism of passage–induced changes is not well understood [7, 16, 17, 21–26]. For example, standard experimental protocols suggest avoiding cells at high passage numbers, whereas the definition of a 'high passage number' is rather vague [7, 25]. On the other hand, the mechanism that causes the seemingly contradictory observations at high passage numbers still remains unknown [16, 17, 21–23]. Computational models can be useful for exploring mechanisms and trade-offs between various factors. Therefore, the problems with high passage numbers invoke us to apply a computational model to investigate putative mechanisms that could lead to the seemingly contradictory changes. As far as we are aware, this is the first time that problems with passaging of cell lines are investigated using a computational approach of this kind.

In this work, we describe a mathematical model that can be used to study the passaging process in 2D *in vitro* cell culture [27, 28]. A key feature of our model is that we allow individual cells within the population to take on a range of characteristics, such as variable proliferation rates, and therefore it is natural to focus on using a discrete model for this purpose [27, 29]. In particular, we are interested in examining whether the apparently contradictory effects of passaging reported in the literature can be recapitulated using a fairly straightforward discrete model. After examining the trade-off between cell heterogeneity and passage–induced damage, we then use the *in silico* model to examine how the passaging process might affect the reproducibility of scratch assays [3, 30]. In this work we focus on the impact of passaging on the cell proliferation rate, and apply a discrete model to explain how passaging can lead to either increasing or decreasing proliferation rates, depending on the competing effects of natural inheritance versus passaging–induced damage. In our model we impose three key assumptions: (i) the passaging process does not affect the cells' ability to migrate; (ii) initially the proliferation rate of each cell is assigned randomly from a normal distribution; and (iii) when proliferating, daughter cells inherit the same proliferation rate as the mother cell. Our approach is to focus on two prototype cell populations. The first is near–homogeneous in the sense that the proliferation rate of the cells is close to constant throughout the population initially. The second has a distinctively heterogeneous distribution of proliferation rates. For each prototype population, we systematically vary the amount of damage caused by passaging to investigate the impact of the damage.

Discrete model

Model framework

We use a discrete random walk model to simulate the passaging process and we refer to individual random walkers in the model as cells. All simulations are performed on a hexagonal

lattice, with the lattice spacing Δ taken to be equal to the average cell diameter [27]. The model includes crowding effects by ensuring that there is, at most, one cell per lattice site [31]. Each lattice site, indexed (i, j) where $i, j \in \mathbb{Z}^+$, has position

$$(x, y) = \begin{cases} \left((i-1)\Delta, \sqrt{3}(j-1)\Delta/2\right) & \text{if } j \text{ is even,} \\ \left((i-1/2)\Delta, \sqrt{3}(j-1)j\Delta/2\right) & \text{if } j \text{ is odd,} \end{cases}$$

such that $1 \leq i \leq I$ and $1 \leq j \leq J$ [27]. In any single realisation of the model, the occupancy of site (i, j) is denoted $C_{i,j}$, with $C_{i,j} = 1$ if the site is occupied, and $C_{i,j} = 0$ if vacant.

If there are $N(t)$ cells at time t, then during the next time step of duration τ, $N(t)$ cells are selected independently at random, one at a time with replacement, and given the opportunity to move [27, 31]. The randomly selected cell attempts to move, with probability P_m, to one of the six nearest neighbour sites, with the target site chosen randomly. Motility events are aborted if a cell attempts to move to an occupied site. Once $N(t)$ potential motility events are attempted, another $N(t)$ cells are selected independently, at random, one at a time with replacement, and given the opportunity to proliferate with probability P_p. The location of the daughter cell is chosen, at random, from one of the six nearest neighbour lattice sites [27, 31]. If the selected lattice site is occupied, the potential proliferation event is aborted. In contrast, if the selected site is vacant, a new daughter cell is placed on that site. After the $N(t)$ potential proliferation events have been attempted, $N(t + \tau)$ is updated [27, 31].

The discrete models in this study are coded in C++, and the simulation code is supplied in S1 Supporting Information.

Simulation domain

The domain is a rectangle of dimensions 10 cm by 7.5 cm, which we use to represent the 75 cm^2 cell culture flask in Fig 1a. This corresponds to a simulation domain in which $I = 4168$ and $J = 3610$, with $\Delta = 24$ μm [3]. Therefore, the maximum number of cells in a 100% confluent monolayer is approximately 15 million. To simplify our visualisation of the model output, although we always perform simulations on the entire 10 cm by 7.5 cm simulation domain, we visualise a smaller, 2 mm by 2 mm, subregion in the centre of the simulation domain, as shown in Fig 1b. No flux boundary conditions along the boundaries of the simulation domain are applied in all cases. For the remainder of this work, we visualise snapshots of the distribution of cells in the smaller field of view, such as the results in Fig 1c and 1d.

Initial condition

Simulations are initiated by randomly populating 15% of lattice sites [6]. At each passage number, the growth of cells in the culture is terminated when 85% confluence is reached. The migration probability P_m of each cell is held constant. Motivated by experimental data of the duration of the mitotic phase for individual cells [32], each cell is initially assigned a random value of P_p, drawn from a normal distribution $\mathcal{N}(\mu_p, \sigma)$ to mimic the stochasticity in proliferation rate among the initial population. When a proliferation event takes place, we invoke the simplest mechanism by assuming that both daughter cells inherit the proliferation rate of the mother cell. For all simulations we set $P_m = 0.35$, $\mu_p = 0.004$, $\Delta = 24$ μm and $\tau = 1/12$ h so that we are considering cell populations with a typical cell diameter, cell diffusivity ($D \approx 600$ μm^2/h) and average proliferation rate ($\lambda \approx 0.05$ /h) [27, 31]. We consider two prototype cell populations: (i) a near–homogeneous cell population with a relatively small variance, $\sigma = 1 \times 10^{-4}$; and (ii) a heterogeneous cell population with a larger variance, $\sigma = 1 \times 10^{-3}$. We choose the values of the standard deviation σ, so that the proliferation rate distribution is within a biologically

reasonable range, and the degree of heterogeneity in the near–homogeneous and heterogeneous cell lines are distinguishable.

Passaging

In our simulations passaging takes place immediately after the population grows to 85% confluence [6]. To split the populations we randomly select a number of cells that is equivalent to cover 15% of lattice sites. These cells are randomly placed on an empty simulation domain to mimic the splitting of cells in the passaging process. Note that P_m is constant for all cells whereas we allow P_p to vary amongst the population and we also assume that the process of passaging the cells involves some damage [21]. Considering that the passaging process involves a combination of chemical (e.g. the usage of trypsin) and mechanical disturbances known to disrupt normal cell behavior, it is reasonable to incorporate some kind of damage mechanism into the passage simulations [6, 15–17, 20–22]. However, the exact cause and the form of the passage–induced damage have not been established. Therefore any form of the passage–induced damage which illustrates certain degrees of stochasticity could be a reasonable choice. In this study, we consider two different degrees of passage–induced damage:

- Small amount of damage: P_p of each cell is decreased by ϵ, where $\epsilon \sim \mathcal{N}(2 \times 10^{-5}, 2 \times 10^{-5})$; and
- Large amount of damage: P_p of each cell is decreased by ϵ, where $\epsilon \sim \mathcal{N}(1 \times 10^{-4}, 1 \times 10^{-4})$.

Each time the population of cells is split, the passage number increases by one. As previous studies indicate that cell proliferation increases at high passage numbers [23], it is possible to assume that the passage–induced damage could lead to the increase in proliferation rate. However, since the aim of this study is to examine the trade-offs between the initial heterogeneity in cell proliferation and the passage–induced damage, in both scenarios we only consider non–negative passage–induced damage by changing any negative damage to zero. This assumption allows us to limit the factors that can increase cell proliferation.

Results and discussion

Passaging cell lines without passage–induced damage

We first investigate how the initial degree of heterogeneity in proliferation rate changes as the passage number increases. In this first set of results we do not consider any form of passage–induced damage. We consider a suite of simulations from passage number 0 to 30 and present results for both the near–homogeneous cell line and the heterogeneous cell line. Snapshots of the field of view at passage number 0 and passage number 30, for both prototype cell populations, are shown in Figs 2a–2d and 3a–3d, respectively. In each snapshot, different colours of cells represent different ranges of the proliferation rate, with red indicating the fastest–proliferating cells and blue showing the slowest–proliferating cells. At the end of passage number 0 we observe a larger variation in cell proliferation rate in the heterogeneous cell line than the near–homogeneous cell line, as we might expect. At the end of passage number 30 we see that there is a dramatic change in the average proliferation rate of cells in the heterogeneous cell line. This change is caused by the fact that cells with higher proliferation rates are more likely to produce daughter cells that directly inherit the higher proliferation rate of the mother cell. Therefore, we observe a greater proportion of faster–proliferating cells in the heterogeneous cell line at high passage number. This leads to a larger average value of P_p and a greater

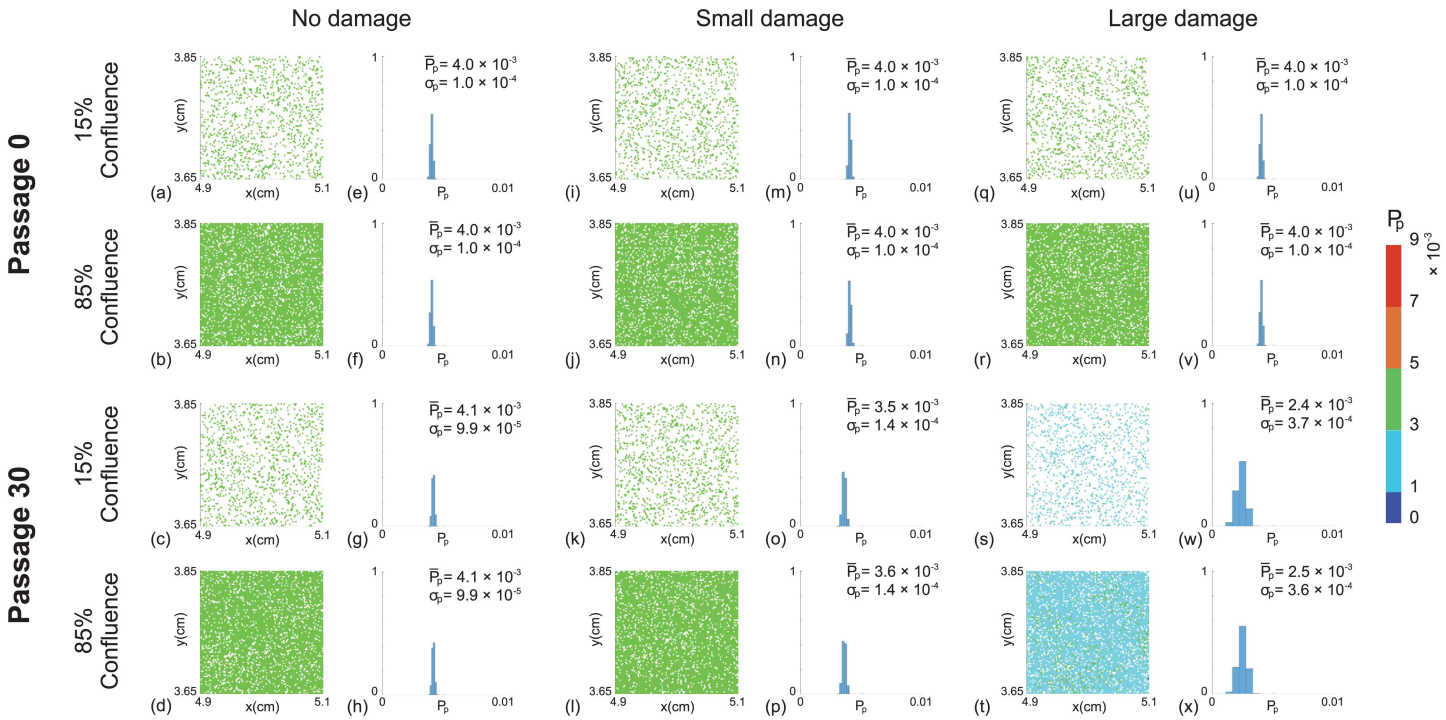

Fig 2. Snapshots of simulations for a near–homogeneous cell line. For each passage number, snapshots at the beginning (15% confluence) and end (85% confluence) of the experiments are shown. Results in (a)–(d), (i)–(l) and (q)–(t) show snapshots of the field of view at passage number 0 and 30, with $\epsilon = 0$, $\epsilon \sim \mathcal{N}(2 \times 10^{-5}, 2 \times 10^{-5})$ and $\epsilon \sim \mathcal{N}(1 \times 10^{-4}, 1 \times 10^{-4})$, respectively. Results in (e)–(h), (m)–(p) and (u)–(x) show distributions of P_p for the entire domain at passage number 0 and 30, with $\epsilon = 0$, $\epsilon \sim \mathcal{N}(2 \times 10^{-5}, 2 \times 10^{-5})$ and $\epsilon \sim \mathcal{N}(1 \times 10^{-4}, 1 \times 10^{-4})$, respectively. The distribution of P_p in each subfigure is obtained from one single realisation. The colour bar indicates P_p for individual cells. $\bar{P}_p$ and σ_p represent the mean and standard deviation of P_p. Each simulation is initiated by randomly populating 15% of lattice sites, on a lattice of size $I = 4168$ and $J = 3610$, with $P_p \sim \mathcal{N}(4 \times 10^{-3}, 1 \times 10^{-4})$ for each cell. All simulations correspond to $\Delta = 24\ \mu$m, $\tau = 1/12$ h, and $P_m = 0.35$.

https://doi.org/10.1371/journal.pone.0181941.g002

variation in P_p across the whole population of cells in the heterogeneous cells line, as shown in Figs 2e–2h and 3e–3h, respectively.

To summarise how the cell proliferation rate changes with passage number, we plot the evolution of the proliferation rate data from the entire populations as boxplots [33] in Fig 4. The boxplots show the median and quartiles of the distribution of P_p from the entire population as a function of the passage number. Comparing results in Fig 4a and 4d shows that the median P_p increases much faster in the heterogeneous cell line than the near–homogeneous cell line. For the near–homogeneous cell line the distribution of P_p appears to be approximately independent of the passage number in this case. In contrast, the distribution of P_p for the heterogeneous cell line is strongly dependent on the passage number. In particular, the median P_p increases, and the distribution of P_p becomes increasingly negatively skewed as the passage number increases. Overall, these results suggest that starting with the same average proliferate rate, the degree of heterogeneity of the cell line alone is enough to lead to very different outcomes when the two cell lines are sufficiently passaged. Therefore, the initial heterogeneity of the cell line appears to be important in terms of understanding how passaging affects properties of cell lines.

In this first set of results, we find that differences in the cell proliferation rate among the cell population can lead to changes in the overall population behaviour at sufficiently high passage numbers. We note that in both prototype cell populations, the average proliferation rate

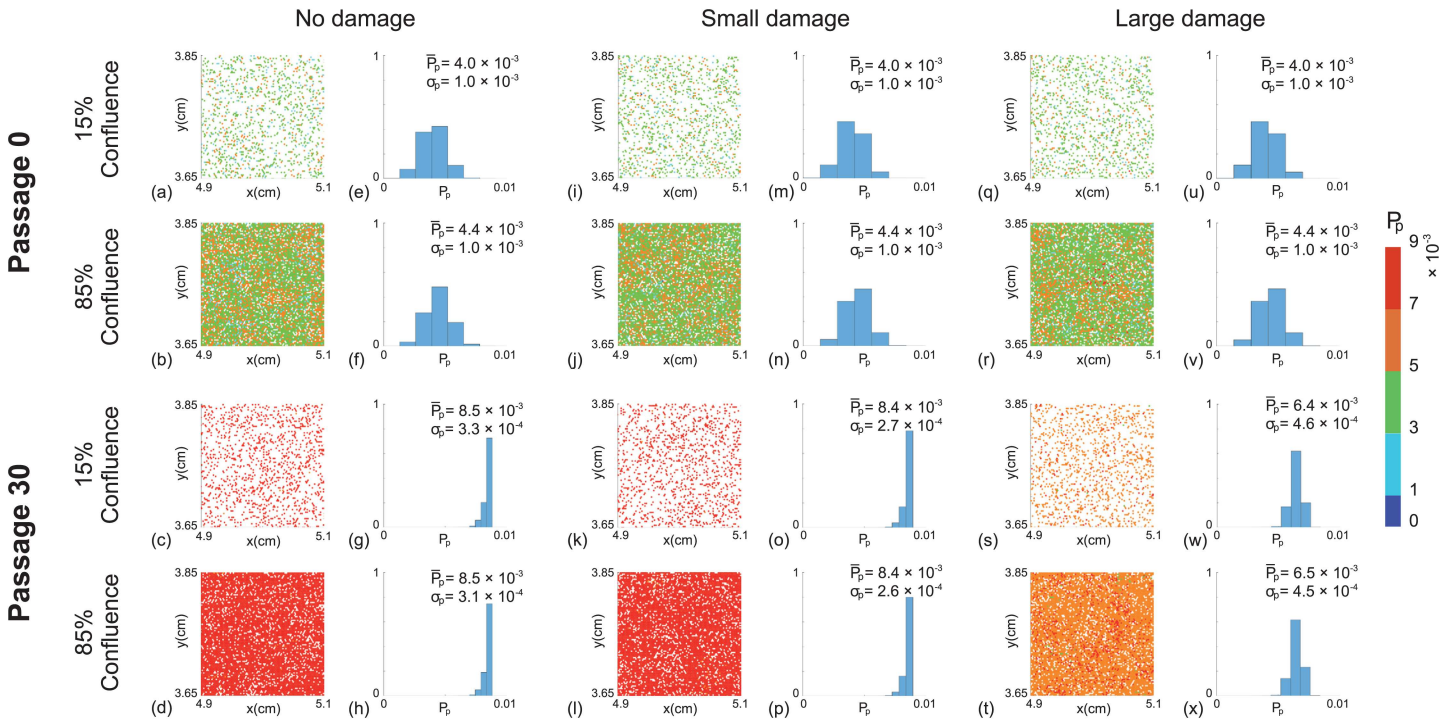

Fig 3. Snapshots of simulations for a heterogeneous cell line. For each passage number, snapshots at the beginning (15% confluence) and end (85% confluence) of the experiments are shown. Results in (a)–(d), (i)–(l) and (q)–(t) show snapshots of the field of view at passage number 0 and 30, with $\epsilon = 0$, $\epsilon \sim \mathcal{N}(2 \times 10^{-5}, 2 \times 10^{-5})$ and $\epsilon \sim \mathcal{N}(1 \times 10^{-4}, 1 \times 10^{-4})$, respectively. Results in (e)–(h), (m)–(p) and (u)–(x) show distributions of P_p for the entire domain at passage number 0 and 30, with $\epsilon = 0$, $\epsilon \sim \mathcal{N}(2 \times 10^{-5}, 2 \times 10^{-5})$ and $\epsilon \sim \mathcal{N}(1 \times 10^{-4}, 1 \times 10^{-4})$, respectively. The distribution of P_p in each subfigure is obtained from one single realisation. The colour bar indicates P_p for individual cells. $\bar{P}_p$ and σ_p represent the mean and standard deviation of P_p. Each simulation is initiated by randomly populating 15% of lattice sites, on a lattice of size $I = 4168$ and $J = 3610$, with $P_p \sim \mathcal{N}(4 \times 10^{-3}, 1 \times 10^{-3})$ for each cell. All simulations correspond to $\Delta = 24$ μm, $\tau = 1/12$ h, and $P_m = 0.35$.

https://doi.org/10.1371/journal.pone.0181941.g003

increases with the passage number and this is consistent with some previous experimental studies [23]. However, most experimental studies report a decrease in average proliferation rate with increasing passage number [16, 17, 21, 22]. This observation motivates us to include a second mechanism in our discrete model, namely passage–induced damage.

Passaging cell lines with passage–induced damage

We now investigate the impact of including passage–induced damage, and we consider both small and large amounts of damage scenarios. All other features of our simulations are maintained as described in the section without passage–induced damage. Snapshots of simulations including small and large amounts of damage, and boxplots showing the distribution of P_p data are shown in Figs 2–4. Comparing results in Fig 2a–2h and 2i–2p suggests that we observe very similar outcomes when we include a small amount of damage in the simulations of the near–homogeneous cell line. Similarly, results in Fig 3a–3h and 3i–3p suggest that the small amount of damage has a negligible impact on the passaging process for the heterogenous cell line. In contrast, with the large amount of damage we see that the proliferation rate decreases by passage number 30 in the near–homogeneous cell line, as shown in Fig 2q–2x, whereas results in Fig 3q–3x show that the proliferation rate increases by passage number 30, but the increase in proliferation rate is not as pronounced as in the case where there is no damage in the heterogenous cell line.

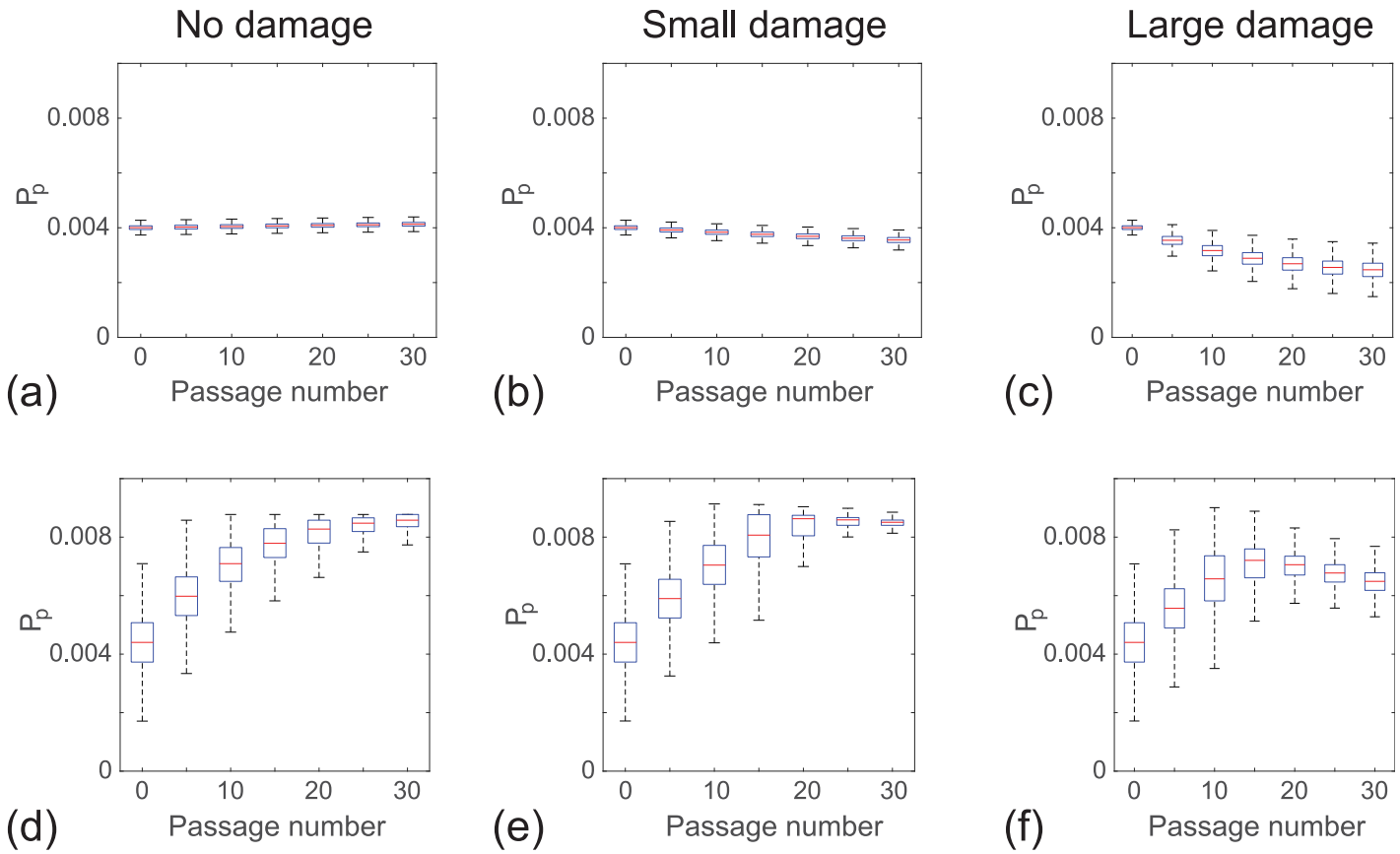

Fig 4. Distribution of P_p as a function of passage number. Results in (a)–(c) show boxplots of P_p for a near–homogeneous cell line at 85% confluence for: (a) no damage $\epsilon = 0$; (b) small amount of damage, $\epsilon \sim \mathcal{N}(2 \times 10^{-5}, 2 \times 10^{-5})$; and (c) large amount of damage, $\epsilon \sim \mathcal{N}(1 \times 10^{-4}, 1 \times 10^{-4})$. Results in (d)–(f) show boxplots of P_p for a heterogeneous cell line at 85% confluence for: (d) no damage $\epsilon = 0$; (e) small amount of damage, $\epsilon \sim \mathcal{N}(2 \times 10^{-5}, 2 \times 10^{-5})$; and (f) large amount of damage, $\epsilon \sim \mathcal{N}(1 \times 10^{-4}, 1 \times 10^{-4})$. In each subfigure the distribution of P_p at individual passage numbers is obtained from one single realisation. Each simulation is initiated by randomly populating 15% of lattice sites on a lattice of size $I = 4168$ and $J = 3610$, with $P_p \sim \mathcal{N}(4 \times 10^{-3}, 1 \times 10^{-4})$ for the near–homogeneous cell line and $P_p \sim \mathcal{N}(4 \times 10^{-3}, 1 \times 10^{-3})$ for the heterogeneous cell line. All simulations correspond to $\Delta = 24$ μm, $\tau = 1/12$ h, and $P_m = 0.35$.

https://doi.org/10.1371/journal.pone.0181941.g004

Results in Figs 2 and 3 focus on snapshots of the population at passage numbers 0 and 30. Additional results in Fig 4b, 4c, 4e and 4f to show how the distribution of P_p evolves as a function of the passage number. For the near–homogeneous cell line, the median P_p decreases monotonically with the passage number for both small and large amounts of damage. In contrast, the median P_p for the heterogeneous cell line behaves very differently as it increases until approximately passage number 20, and then decreases with further passaging. These results, combined, provide a simple explanation for why some previous studies have reported that the proliferation rate can increase with passage number, as in the case of Fig 4d and 4e, whereas other studies suggest that the proliferation rate can decrease with passage number, as in the case of Fig 4c. In fact, our results suggest that it is possible to have a situation where the proliferation rate both increases and decreases with passage number, as in the case of Fig 4f, and we observe different trends depending on the passage number. These differences arise in our model due to a trade-off between the initial heterogeneity of the cell line and the amount of damage sustained in the passaging process.

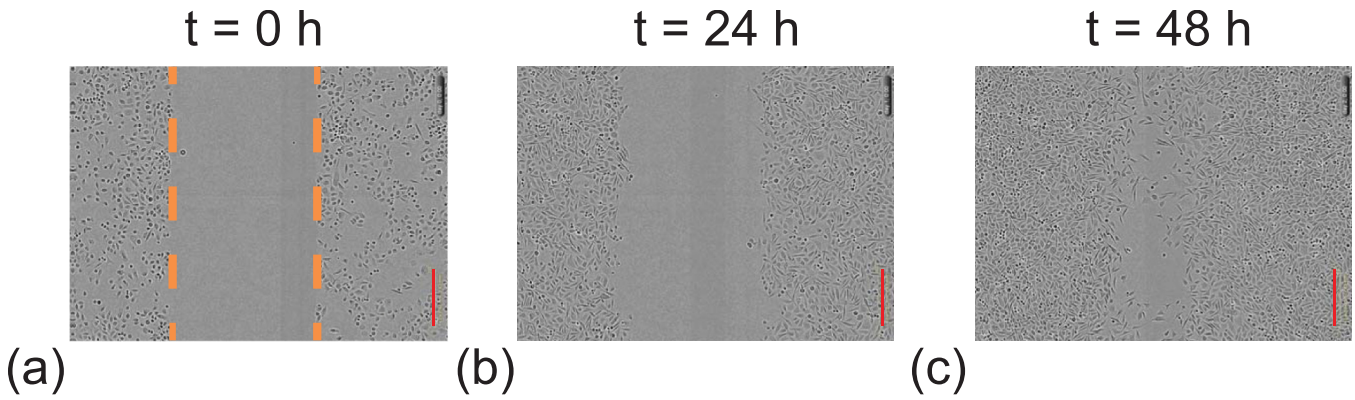

Fig 5. Experimental images of an IncuCyte ZOOM™ scratch assay [3, 38]. The images in (a)–(c) show the closure of the initially scratched region which is highlighted by the dashed orange lines at $t = 0$. The red scale bar corresponds to 300 μm. These images are reproduced, with permission [3].

https://doi.org/10.1371/journal.pone.0181941.g005

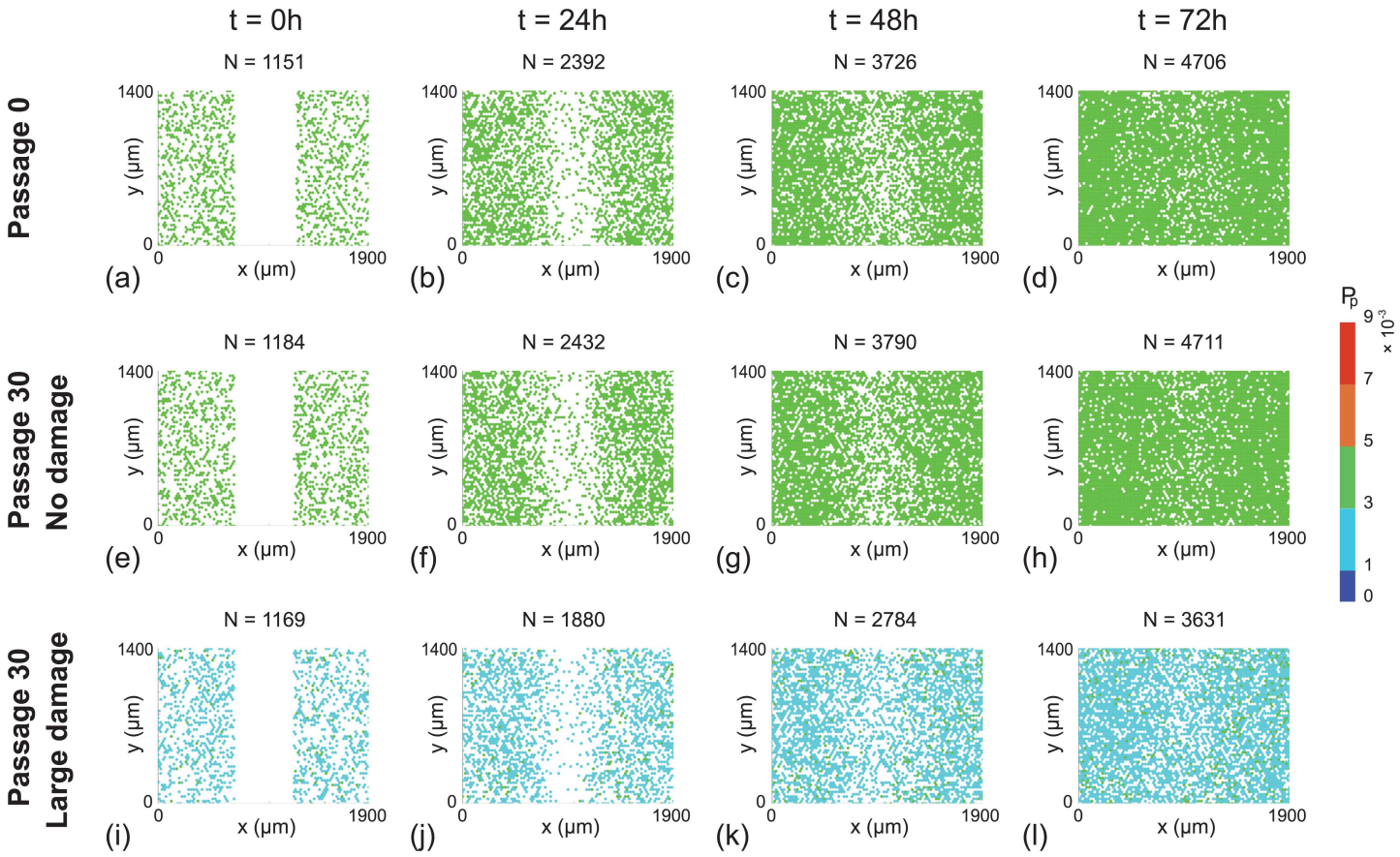

Fig 6. Snapshots of a suite of scratch assays performed using a near–homogeneous cell line. In each column the distributions of cells at time $t = 0$, 24, 48, 72 h are shown. Each simulation is initiated by randomly populating a lattice of size 80 × 68, so that each site is occupied with probability 30%. A scratch of 23 lattice sites wide is made at $t = 0$ h. All simulations correspond to $\Delta = 24$ μm, $\tau = 1/12$ h, and $P_m = 0.35$. In each row the initial P_p of individual cells is assigned by randomly selecting from the *in silico* data in Fig 2f, 2h and 2x, respectively.

https://doi.org/10.1371/journal.pone.0181941.g006

Scratch assay with passaged cells

Having demonstrated that the interplay between cell heterogeneity and passage–induced damage can lead to complicated trends in the relationship between the proliferation rate and passage number, it is still unclear how these kinds of differences can affect how we interpret *in vitro* experiments. To explore this issue we use cells from a range of passage conditions to mimic a scratch assay [30]. For this purpose we focus on the geometry associated with experimental images obtained from an IncuCyte ZOOM™ scratch assay [3, 34–37], as shown in Fig 5. The images, of dimension 1400 μm × 1900 μm, show a fixed field of view that is much smaller than the spatial extent of the cells in the scratch assay [27, 38]. To model this situation we apply zero net flux boundary conditions along all boundaries of the lattice. We use a lattice of size 80 × 68 to accommodate a typical population of cells with $\Delta = 24$ μm. To initialise the scratch assay, we randomly populate all lattice sites with an equal probability of 30% [3]. To simulate the scratch, we remove all cells from a vertical strip of width approximately 550 μm, and we then observe the rate at which the populations spread into the vacant area. All cells have the same constant value of $P_m = 0.35$, and we assign values of P_p by sampling from the various histograms in Figs 2 and 3. This means that we are effectively simulating a scratch assay using cells from different cell lines, with different amounts of passage-induced damage,

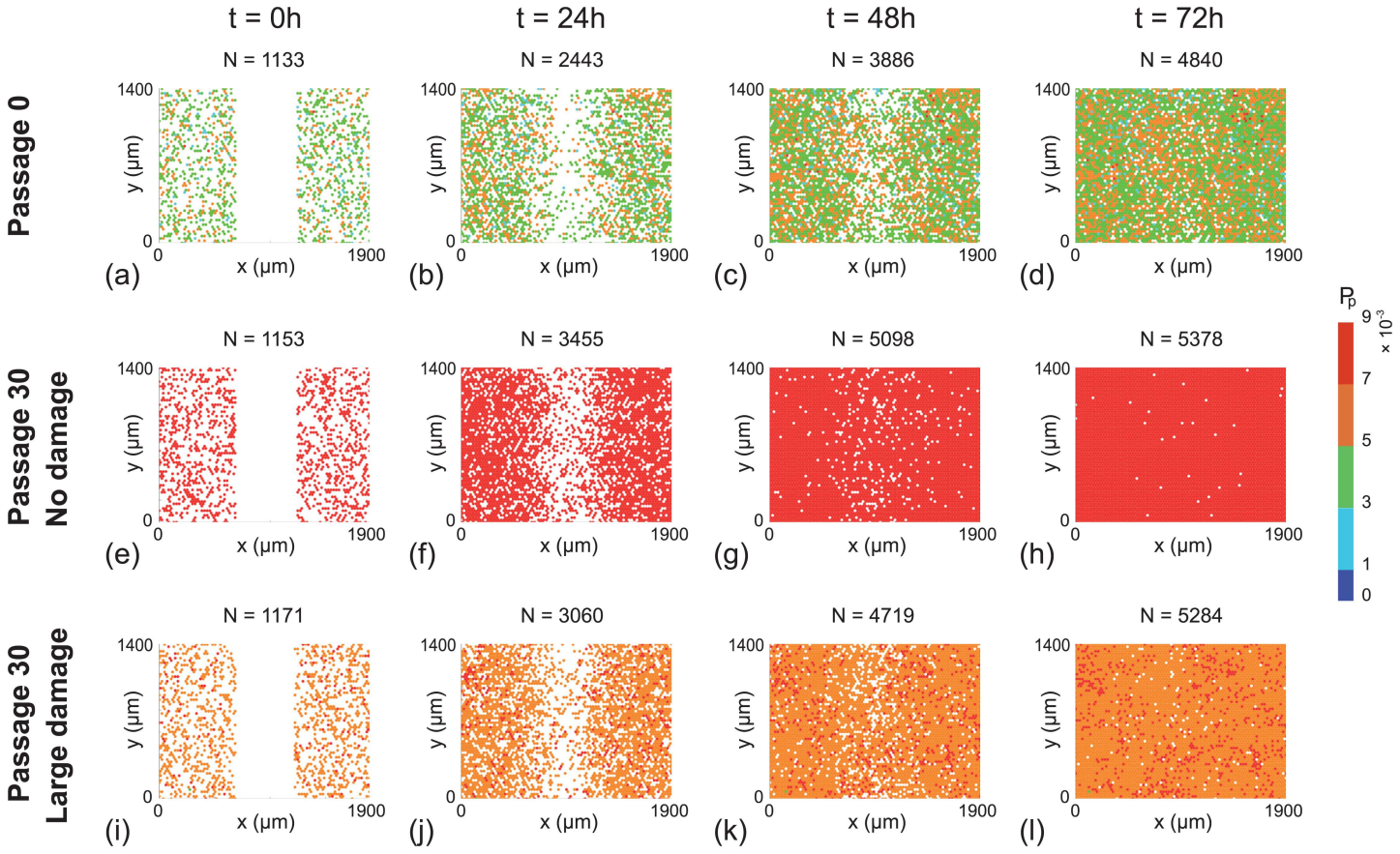

Fig 7. Snapshots of a suite of scratch assays performed using a heterogeneous cell line. In each column the distributions of cells at time $t = 0$, 24, 48, 72 h are shown. Each simulation is initiated by randomly populating a lattice of size 80 × 68, so that each site is occupied with probability 30%. A scratch of 23 lattice sites wide is made at $t = 0$ h. All simulations correspond to $\Delta = 24$ μm, $\tau = 1/12$ h, and $P_m = 0.35$. In each row the initial P_p of individual cells is assigned by randomly selecting from the *in silico* data in Fig 3f, 3h and 3x, respectively.

https://doi.org/10.1371/journal.pone.0181941.g007

and from different passage numbers according to our *in silico* results of cell culture growth in the previous section.

Snapshots from the discrete model, showing the progression of the scratch assays, are shown in Figs 6 and 7. In general we see that, regardless of the initial cell population, all of the scratch assays lead to successful closure by approximately 48–72 h, which is consistent with standard experimental observations [3, 35]. However, close examination of the results reveals some differences. In particular, visual inspection of the snapshots suggests that those cell populations with higher initial proliferation rate lead to larger numbers of cells at later times, and hence more rapid closure of the initially–vacant space. These trends are subtle, but are most obvious in Fig 7 where the population corresponds to cells taken from passage number 30, with no damage, leading to more effective re-colonisation of the initially–vacant space than cells from passage number 0. Since these differences are subtle it may be difficult to detect them when visually comparing results from scratch assays. Therefore, we will

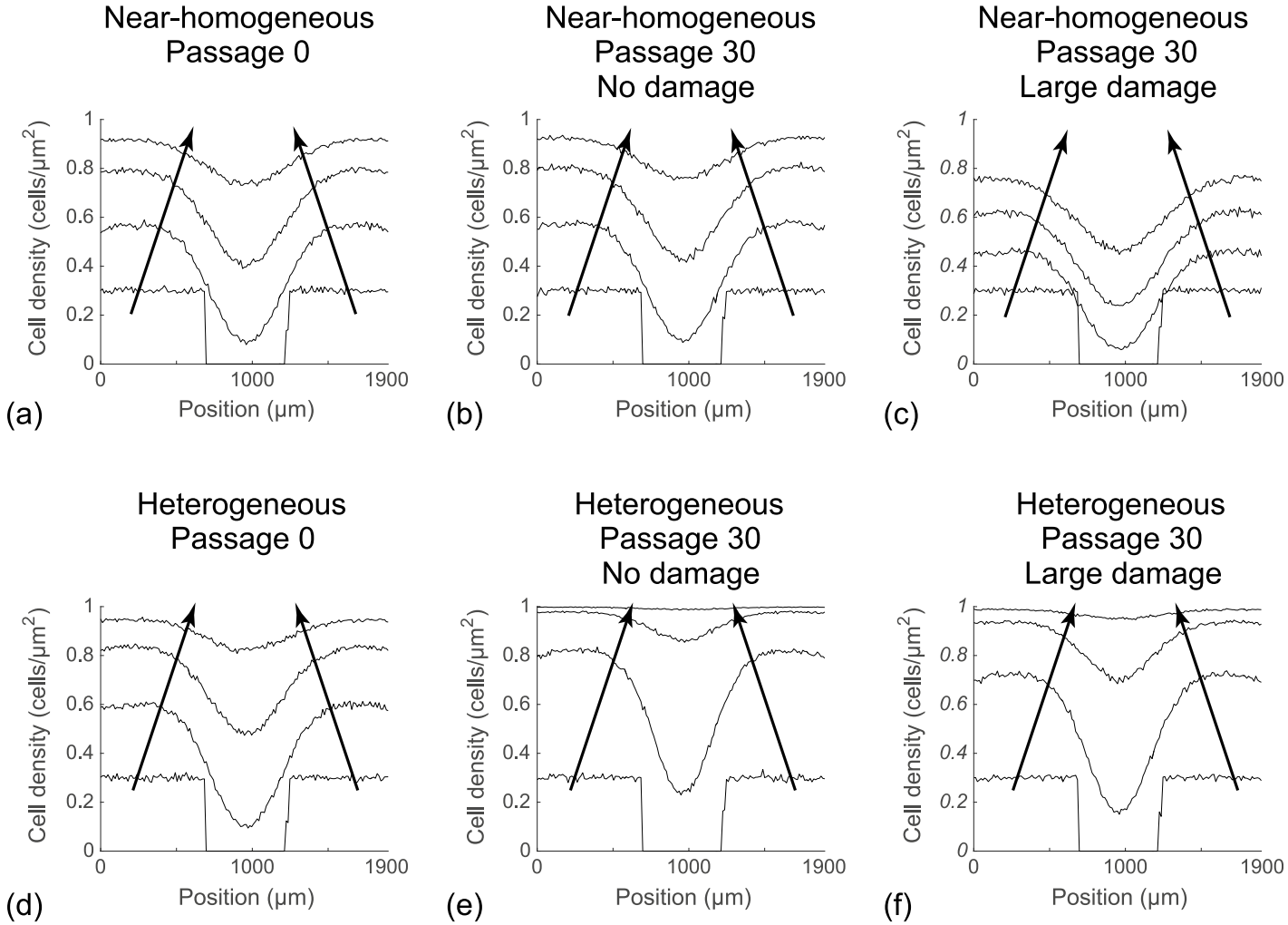

Fig 8. Averaged simulation data showing cell density profiles from the scratch assays. (a)–(c): Cell density profiles for a near–homogeneous cell line. (d)–(f): Cell density profiles for a heterogeneous cell line. In each subfigure cell density profiles are given at $t = 0$, 24, 48, 72 h, and the direction of increasing t is shown with the arrows. All simulation results are averaged across 100 identically prepared realisations of the discrete model, with $\Delta = 24\ \mu$m, $\tau = 1/12$ h, and $P_m = 0.35$, on a lattice of size 80 × 68. In each subfigure the initial P_p of individual cells is assigned by randomly selecting from the corresponding *in silico* data in Figs 2f, 2h, 2x and 3f, 3h and 3x, respectively.

https://doi.org/10.1371/journal.pone.0181941.g008

now quantify the spatial and temporal distribution of cells in Figs 6 and 7 to provide more information.

Since the initial condition is uniform in the vertical direction [27, 31], we average the population density in Figs 6 and 7 along each vertical column of lattice sites to obtain

$$\langle C_i \rangle = \frac{1}{J}\sum_{j=1}^{J} C_{i,j}.$$

This quantity is further averaged by considering 100 identically prepared simulations of the discrete model to reduce fluctuations [27]. This procedure allows us to plot the time evolution of the average cell density as a function of the horizontal coordinate, as shown in Fig 8 [27]. Results in Fig 8a–8b suggest that the evolution of the cell density profile is practically indistinguishable when we consider cells from the near–homogeneous cell line that is passaged without damage, as we might expect from the results in Fig 4a. In contrast, comparing results in Fig 8a with results in Fig 8c shows that we observe very different results when damage is included in the passaging process for the near–homogeneous cell line. When we consider the results in Fig 8d–8f, for the heterogeneous cell line, we see that the evolution of the cell density profiles is very different for all three cases considered.

Conclusion

Passaging of cell lines is an essential processes of growing cells in cell culture [6, 7]. The passaging process involves both chemical and mechanical disturbances which accumulatively change cell characteristics. Problems associated with high passage numbers, such as the change of cell proliferation, are widely acknowledged. However, the mechanisms are not well understood [16, 17, 21–26]. Therefore, the aim of this work is to use a computational approach to provide insight into the putative mechanisms that could possibly lead to the problems.

In this work, we apply a lattice–based discrete model to investigate and quantify the impact of passaging cell lines. Although there are many properties of cells that are affected by the passaging process [15–17, 20–22, 24, 26], we choose to focus on how passaging affects the cell proliferation rate. In our model, when a cell proliferates, the daughter cells directly inherit the same proliferation rate as the mother cell. Furthermore, we also assume that during the passaging process, the cell proliferation rate is decreased by some passage–induced damage. For all results presented, we investigate the role of cell heterogeneity by comparing results where we begin the passaging process with a hear-homogeneous population of cells where P_p is almost constant, with a heterogeneous population of cells where P_p varies significantly among the population.

In the literature, previous experimental studies have reported apparently contradictory results where some studies suggest that the average proliferation rate of cells can increase at large passage number [23], whereas other studies suggest that the average proliferation rate of cells can decrease with passage number [16, 17, 21, 22]. We find that by varying the competition between passage-induced damage and cell heterogeneity, our relatively straightforward simulation model can predict each of these outcomes.

To study how passage number can affect *in vitro* experiments, we simulate a suite of scratch assays using various populations of cells that are harvested from our *in silico* passaging process. Our simulation results show that the passage number can lead to subtle changes in the evolution of the scratch assay and these changes might be very difficult to detect visually. We provide additional information about how the distribution of cells in a scratch assay might be influenced by passage number by performing a large number of realisations and examining the average cell density profiles. These average cell density profiles make it obvious that the

passage number could affect the rate of scratch closure. This observation, together with the fact that cell passage number is often unreported in the experimental literature [12, 13], could explain why scratch assays are notoriously difficult to reproduce [39]. In addition, the results of cell culture growth and scratch assays indicate that even at the same passage number, the initial heterogeneity in cell proliferation can give rise to very differently behaving cell populations. Therefore, separating cell population without reporting the proliferative capacity can also affect the reproducibility of *in vitro* experiments. However, the proliferative capacity of cell lines can be difficult to measure experimentally, as most of the previous experiments only report the cell population evolution [17, 23], or the duration of the cell cycle [32].

There are several implications of this study that could be of interest to the experimental community. First, we suggest that the passage number of cell lines should always be reported. Second, there is a need for more experimental evidence about the impact of passaging on proliferation rates of various cell lines. For example, careful measurements of proliferation rates over a sequence of passage numbers would provide more insight into the variability of key cell properties in cell culture. This type of quantitative information would be invaluable for understanding reproducibility of standard *in vitro* experiments. Third, we acknowledge that our choices of the standard deviation, σ, to define the spread of the distribution of proliferation rates in the near–homogeneous and heterogeneous cell lines is rather theoretical. Recently, Haass et al. have devised new experimental methods that can be used to measure the durations of different phases in cell cycle for a range of melanoma cell lines [32]. This data could be used used to estimate the properties of the distribution of cell proliferation rates, such as the mean and standard deviation of the distribution of proliferation rates. Therefore, we suggest that similar experiments could be performed to generate proliferation rate distribution over various passage numbers for a range of different cell lines of interest. This data could then be directly integrated within our *in silico* models to examine the interplay between the degree of heterogeneity and passage–induced damage.

There are also several implications of this study that are of interest to the applied mathematics and mathematical biology communities. First, here we focus on the case where there is heterogeneity in the rate at which individual cells proliferate in the population but, we treat the motility rate as a constant. This is because most previous experimental studies have reported differences in the rate of proliferation as a function of passage number rather than differences in the rate of migration [17, 22, 23]. However, heterogeneity in cell migration rate can also affect the reproducibility of *in vitro* experiments [21], especially scratch assays in which cell migration plays a key role in wound closure [3]. An interesting extension of our present study would involve dealing with both variability in the motility rate and the proliferation rate [40]. Second, in our work we make the most straightforward assumption that daughter cells inherit P_p directly from the mother cell. It might be more plausible to introduce some stochasticity in the inheritance process, and it might also be plausible to incorporate some kind of ageing process where the proliferation depends on the age structure of the population [21]. We have chosen not to include these additional details as we wish to present a simpler model that is capable of illustrating a proof–of–principle concept rather than capturing every possible feature of the underlying biology. Finally, another extension of this work would be to consider the derivation of an accurate mean–field approximation that could be used to describe the evolution of the cell density profiles in Fig 7. This is a challenging task because all previous derivations of such mean–field partial differential equations involve populations of cells with constant rates [27, 31, 41–45], whereas we are dealing with a more realistic heterogeneous population of cells.

Supporting information

S1 Supporting Information. C++ simulation code.
(PDF)

Acknowledgments

This work is funded by the Australian Research Council (Grants: DP140100249 to MJS and SWM, DP170100474 to MJS; http://www.arc.gov.au/). The funders had no role in study design, data collection, decision to publish, or preparation of the manuscript.

Author Contributions

Conceptualization: Wang Jin, Catherine J. Penington, Scott W. McCue, Matthew J. Simpson.

Data curation: Wang Jin.

Formal analysis: Wang Jin, Catherine J. Penington, Scott W. McCue, Matthew J. Simpson.

Funding acquisition: Scott W. McCue, Matthew J. Simpson.

Investigation: Wang Jin, Catherine J. Penington, Scott W. McCue, Matthew J. Simpson.

Methodology: Wang Jin, Catherine J. Penington, Scott W. McCue, Matthew J. Simpson.

Project administration: Scott W. McCue, Matthew J. Simpson.

Resources: Scott W. McCue, Matthew J. Simpson.

Software: Wang Jin.

Supervision: Catherine J. Penington, Scott W. McCue, Matthew J. Simpson.

Validation: Wang Jin.

Visualization: Wang Jin.

Writing – original draft: Wang Jin, Catherine J. Penington, Scott W. McCue, Matthew J. Simpson.

Writing – review & editing: Wang Jin, Catherine J. Penington, Scott W. McCue, Matthew J. Simpson.

References

1. Abbott A. Cell culture: biology's new dimension. Nature. 2003; 424: 870–872. https://doi.org/10.1038/424870a PMID: 12931155
2. Frascoli F, Hughes BD, Zaman MH, Landman KA. A computational model for collective cellular motion in three dimensions: general framework and case study for cell pair dynamics. PLOS ONE. 2013; 8: e59249. https://doi.org/10.1371/journal.pone.0059249 PMID: 23527148
3. Jin W, Shah ET, Penington CJ, McCue SW, Chopin LK, Simpson MJ. Reproducibility of scratch assays is affected by the initial degree of confluence: Experiments, modelling and model selection. J Theor Biol. 2016; 390: 136–145. https://doi.org/10.1016/j.jtbi.2015.10.040 PMID: 26646767
4. Kisiday J, Jin M, Kurz B, Hung H, Semino C, Zhang S, et al. Self-assembling peptide hydrogel fosters chondrocyte extracellular matrix production and cell division: implications for cartilage tissue repair. P Natl Acad Sci USA. 2002; 99: 9996–10001. https://doi.org/10.1073/pnas.142309999
5. Vichai V, Kirtikara K. Sulforhodamine B colorimetric assay for cytotoxicity screening. Nat Protoc. 2006; 1:1112–1116. https://doi.org/10.1038/nprot.2006.179 PMID: 17406391
6. ATCC. Thawing, propagating, and cryopreserving protocol NCI–PBCF–CRL1435 (PC–3) Prostate Adenocarcinoma (ATCCCRL-1435™). ATCC. 2012. Available from: http://physics.cancer.gov/docs/bioresource/prostate/NCI-PBCF-CRL1435_PC-3_SOP-508.pdf. (Accessed July 2017).

7. ATCC. Passage number effects in cell lines. ATCC. 2016. Available from: https://www.atcc.org/~/media/PDFs/Technical%20Bulletins/tb07.ashx. (Accessed July 2017).
8. Haridas P, Penington CJ, McGovern JA, McElwain DLS, Simpson MJ. Quantifying rates of cell migration and cell proliferation in co–culture barrier assays reveals how skin and melanoma cells interact during melanoma spreading and invasion. J Theor Biol. 2017; 423: 13–25. https://doi.org/10.1016/j.jtbi.2017.04.017 PMID: 28433392
9. Treloar KK, Simpson MJ. Sensitivity of edge detection methods for quantifying cell migration assays. PLOS ONE. 2013; 8: e67389. https://doi.org/10.1371/journal.pone.0067389 PMID: 23826283
10. Treloar KK, Simpson MJ, Haridas P, Manton KJ, Leavesley DI, McElwain DLS, et al. Multiple types of data are required to identify the mechanisms influencing the spatial expansion of melanoma cell colonies. BMC Syst Biol. 2013; 7: 137. https://doi.org/10.1186/1752-0509-7-137 PMID: 24330479
11. Treloar KK, Simpson MJ, McElwain DLS, Baker RE. Are *in vitro* estimates of cell diffusivity and cell proliferation rate sensitive to assay geometry? J Theor Biol. 2014; 356: 71–84. https://doi.org/10.1016/j.jtbi.2014.04.026 PMID: 24787651
12. Vasilevsky NA, Brush MH, Paddock H, Ponting L, Tripathy SJ, LaRocca GM, et al. On the reproducibility of science: unique identification of research resources in the biomedical literature. PeerJ. 2013; 1: e148. https://doi.org/10.7717/peerj.148 PMID: 24032093
13. Allegrucci C, Young LE. Differences between human embryonic stem cell lines. Hum Reprod Update. 2007; 13: 103–120. https://doi.org/10.1093/humupd/dml041 PMID: 16936306
14. Haridas P, McGovern JA, Kashyap AS, McElwain DLS, Simpson MJ. Standard melanoma–associated markers fo not identify the MM127 metastatic melanoma cell line. Sci Rep. 2016; 6: 24569. https://doi.org/10.1038/srep24569 PMID: 27087056
15. Cooley C, Baird KM, Faure V, Wenner T, Stewart JL, Modino S, et al. Trf1 is not required for proliferation or functional telomere maintenance in chicken DT40 cells. Mol Biol Cell. 2009; 20: 2563–2571. https://doi.org/10.1091/mbc.E08-10-1019 PMID: 19321665
16. Foster SA, Galloway DA. Human papillomavirus type 16 E7 alleviates a proliferation block in early passage human mammary epithelial cells. Oncogene. 1996; 12: 1773–1779. PMID: 8622898
17. Hayflick L. The limited *in vitro* lifetime of human diploid cell strains. Exp Cell Res. 1965; 37: 614–636. https://doi.org/10.1016/0014-4827(65)90211-9 PMID: 14315085
18. Kippin TE, Martens DJ, van der Kooy D. p21 loss compromises the relative quiescence of forebrain stem cell proliferation leading to exhaustion of their proliferation capacity. Gene Dev. 2005; 19: 756–767. https://doi.org/10.1101/gad.1272305 PMID: 15769947
19. Laurent LC, Ulitsky I, Slavin I, Tran H, Schork A, Morey R, et al. Dynamic changes in the copy number of pluripotency and cell proliferation genes in human ESCs and iPSCs during reprogramming and time in culture. Cell Stem Cell. 2011; 8: 106–118. https://doi.org/10.1016/j.stem.2010.12.003 PMID: 21211785
20. Pfeiffer MJ, Schalken JA. Stem cell characteristics in prostate cancer cell lines. Eur Urol. 2010; 57: 246–255. https://doi.org/10.1016/j.eururo.2009.01.015 PMID: 19200636
21. Rubin H. Cell aging *in vivo* and *in vitro*. Mech Ageing Dev. 1997; 98: 1–35. https://doi.org/10.1016/S0047-6374(97)00067-5 PMID: 9255755
22. Schneider EL, Mitsui Y. The relationship between in vitro cellular aging and *in vivo* human age. P Natl Acad Sci USA. 1976; 73: 3584–3588. https://doi.org/10.1073/pnas.73.10.3584
23. Lin HK, Hu YC, Yang L, Altuwaijri S, Chen YT, Kang HY, et al. Suppression versus induction of androgen receptor functions by the phosphatidylinositol 3-kinase/Akt pathway in prostate cancer LNCaP cells with different passage numbers. J Biol Chem. 2003; 278: 50902–50907. https://doi.org/10.1074/jbc.M300676200 PMID: 14555644
24. Gracia JC, Van den Hoecke S, Saelens X, Van Reeth K. Effect of serial pig passages on the adaptation of an avian H9N2 influenza virus to swine. PLOS ONE. 2017; 12: e0175267. https://doi.org/10.1371/journal.pone.0175267
25. Public Health England. Passage numbers explained. Public Health England. 2017. Available from: https://www.phe-culturecollections.org.uk/media/114565/m219_passage-numbers-explained.pdf. (Accessed July 2017).
26. Zhang H, Zhu NX, Huang K, Cai BZ, Zeng Y, Xu YM, et al. iTRAQ–Based Quantitative Proteomic Comparison of Early–and Late–Passage Human Dermal Papilla Cell Secretome in Relation to Inducing Hair Follicle Regeneration. PLOS ONE. 2016; 11: e0167474. https://doi.org/10.1371/journal.pone.0167474 PMID: 27907131
27. Jin W, Penington CJ, McCue SW, Simpson MJ. Stochastic simulation tools and continuum models for describing two–dimensional collective cell spreading with universal growth functions. Phys Biol. 2016; 13: 056003. https://doi.org/10.1088/1478-3975/13/5/056003 PMID: 27716634

28. Vo BN, Drovandi CC, Pettitt AN, Simpson MJ. Quantifying uncertainty in parameter estimates for stochastic models of collective cell spreading using approximate Bayesian computation. Math Biosci. 2015; 263: 133–142. https://doi.org/10.1016/j.mbs.2015.02.010 PMID: 25747415

29. Dunn SJ, Osborne JM, Appleton PL, Näthke I. Combined changes in Wnt signaling response and contact inhibition induce altered proliferation in radiation–treated intestinal crypts. Mol Biol Cell. 2016; 27: 1863–1874. https://doi.org/10.1091/mbc.E15-12-0854 PMID: 27053661

30. Liang CC, Park AY, Guan JL. *In vitro* scratch assay: a convenient and inexpensive method for analysis of cell migration *in vitro*. Nat Protoc. 2007; 2: 329–333. https://doi.org/10.1038/nprot.2007.30 PMID: 17406593

31. Simpson MJ, Landman KA, Hughes BD. Cell invasion with proliferation mechanisms motivated by time–lapse data. Physica A. 2010; 389: 3779–3790. https://doi.org/10.1016/j.physa.2010.05.020

32. Haass NK, Beaumont KA, Hill DS, Anfosso A, Mrass P, Munoz MA, et al. Real–time cell cycle imaging during melanoma growth, invasion, and drug response. Pigm Cell Melanoma R. 2014; 27: 764–776. https://doi.org/10.1111/pcmr.12274

33. MathWorks. Boxplot. 2016. Available from: https://au.mathworks.com/help/stats/boxplot.html. (Accessed July 2017).

34. Gao Y, Theng SS, Zhuo J, Teo WB, Ren J, Lee CG (2014). FAT10, an ubiquitin–like protein, confers malignant properties in non–tumorigenic and tumorigenic cells. Carcinogenesis. 35: 923–934. https://doi.org/10.1093/carcin/bgt407 PMID: 24325913

35. Gujral TS, Chan M, Peshkin L, Sorger PK, Kirschner MW, MacBeath G. A noncanonical Frizzled2 pathway regulates epithelial–mesenchymal transition and metastasis. Cell. 2014; 159: 844–856. https://doi.org/10.1016/j.cell.2014.10.032 PMID: 25417160

36. Ruttala HB, Ko YT. Liposomal co-delivery of curcumin and albumin/paclitaxel nanoparticle for enhanced synergistic antitumor efficacy. Colloid Surface B. 2015; 128: 419–426. https://doi.org/10.1016/j.colsurfb.2015.02.040

37. Yang Q, Jia C, Wang P, Xiong M, Cui J, Li L, et al. MicroRNA–505 identified from patients with essential hypertension impairs endothelial cell migration and tube formation. Int J Cardiol. 2014; 177: 925–934. https://doi.org/10.1016/j.ijcard.2014.09.204 PMID: 25449503

38. Jin W, Shah ET, Penington CJ, McCue SW, Maini PK, Simpson MJ. Logistic proliferation of cells in scratch assays is delayed. Bull Math Biol. 2017; 79: 1028–1050. https://doi.org/10.1007/s11538-017-0267-4 PMID: 28337676

39. Gough W, Hulkower KI, Lynch R, Mcglynn P, Uhlik M, Yan L, et al. A quantitative, facile, and high–throughput image–based cell migration method is a robust alternative to the scratch assay. J Biomol Screen. 2011; 16: 155–163. https://doi.org/10.1177/1087057110393340 PMID: 21297103

40. Petrovskii S, Mashanova A, Jansen VAA. Variation in individual walking behaviour creates the impression of a Levy flight. P Natl Acad Sci USA. 2011; 108: 8704–8707. https://doi.org/10.1073/pnas.1015208108

41. Dale PD, Maini PK, Sherratt JA. Mathematical modelling of corneal epithelial wound healing. Math Biosci. 1994; 124: 127–147. https://doi.org/10.1016/0025-5564(94)90040-X PMID: 7833592

42. Mahasa KJ, Ouifki R, Eladdadi A, de Pillis L. Mathematical model of tumor–immune surveillance. J Theor Biol. 2016; 404: 312–330. https://doi.org/10.1016/j.jtbi.2016.06.012 PMID: 27317864

43. Sengers BG, Please CP, Oreffo ROC. Experimental characterization and computational modelling of two–dimensional cell spreading for skeletal regeneration. J R Soc Interface. 2007; 4: 1107–1117. https://doi.org/10.1098/rsif.2007.0233 PMID: 17472907

44. Tsoularis A, Wallace J. Analysis of logistic growth models. Math Biosci. 2002; 179: 21–55. https://doi.org/10.1016/S0025-5564(02)00096-2 PMID: 12047920

45. Simpson MJ, Landman KA, Hughes BD. Pathlines in exclusion processes. Phys Rev E. 2009; 79: 031920. https://doi.org/10.1103/PhysRevE.79.031920